

EVALUATION OF A ROAD SIGN PRE-DETECTION SYSTEM BY IMAGE ANALYSIS

Philippe Foucher, Pierre Charbonnier and Housseem Kebbous

ERA 27 LCPC, Laboratoire des Ponts et Chaussées, 11 rue Jean Mentelin, B.P. 9, 67035 Strasbourg, France

Keywords: Image analysis, Road sign detection, Road sign inventory, Color, Shape, Symmetry, Evaluation.

Abstract: In this paper, we introduce a pre-detection algorithm dedicated to French danger-warning and prohibitory road signs. The proposed method combines color, shape, location and symmetry features to select among large image databases, a small subset of pictures that probably contain road signs. We report the results of a systematic experimental assessment that we performed on five image databases, comprised of more than 26,000 images, covering 176 km and containing 371 traffic signs, among which a non-negligible amount (about 5% in average) is damaged. The experiments show that about 10% images of the sequences are selected and more than 87% traffic signs are detected. The missed objects always correspond to dirty, worn-out or badly oriented signs that would be difficult to detect even for a human operator.

1 INTRODUCTION

In this paper, we address the problem of road sign inventory. In our application, evenly spaced still-images of the roadway and its close surroundings (see e.g. Fig. 1) are collected by inspection vehicles along itineraries, typically one image every 5 or 10 meters. These image databases are then processed *off-line* by human operators, which is fastidious and prone to oversights. Our research aims at proposing image analysis tools for automating the operator's task. In particular, it may be useful to select, among all the data set, the small number (typically, 5 to 10 %) of images that probably contain road signs. We propose in this paper such a *pre-detection* procedure, that relies on color, shape, location and symmetry features. The algorithm is described in the case of French danger-warning and prohibitory signs, which are red, but may readily be extended to other types of colored road signs. The second contribution of the paper is that we perform a systematic and objective evaluation of the pre-selection procedure on large image databases, taken by various cameras.

The paper is organized as follows. We first propose a brief review of related work (Sect. 2). Then, Sect. 3 describes the three steps of the pre-detection algorithm. Sect. 4 presents the experimental setup and in Sect. 5 we comment the experimental results.

2 RELATED WORK

Traffic sign detection and recognition by image analysis are useful for many applications such as road sign inventory, driving assistance or autonomous systems. In the last two decades, many research teams have been interested in this topic, see e.g. (Barnes et al., 2008) for a recent survey. Detection methods generally rely on the fact that road signs are manufactured, standardized objects, whose shape, dimensions, color and location are fixed by norms. However, detection systems encounter typical problems of computer vision in uncontrolled environments, such as: variations in lighting conditions (brightness, reflections, shadows...), geometric distortions (rotations), complexity of road scenes (neighboring objects with similar color, occlusions), object's wear and tear. In many researches, the detection system uses a combination of color and shape information. Color-based segmentation is commonly applied first, to extract pixels corresponding to the color of the road sign. The Hue component, which is not sensitive to lighting changes, is usually used for this task (Shaposhnikov et al., 2002; de la Escalera et al., 2003). However, an efficient alternative is to consider the normalized component $R/(R + G + B)$ which is also independent on lighting changes (Dutilleux and Charbonnier, 2007). Secondly, the connected components are selected according to some shape parameters, e.g. size of the object area (Maldonado-Bascon et al., 2007), geometri-

cal properties of edge segments (Piccioli et al., 1996) (note that in (Piccioli et al., 1996), the robustness of the shape detector to occlusions is not discussed).

Some authors directly work with grey-level images to avoid the difficulties of color-based segmentation. For instance, (Loy and Barnes, 2004) adapt the Fast Radial Symmetry detector described by (Loy and Zelinsky, 2003) to the detection of regular polygon.

This paper presents a systematic evaluation of the performance of the pre-detection algorithm on different sets of sequences. In the literature, the evaluation of road sign detectors often concerns only a limited number of images and/or situations. To our knowledge, quantitative evaluation on a large database was only performed in (Priese et al., 1993). In this project, a detection and recognition algorithm was tested on 20000 images and the performance were given in terms of true detections and false alarms. More recently, (Barnes et al., 2008) uses the Receiving Operating Characteristic (ROC) curves to perform a systematic evaluation of a detection and recognition algorithm.

3 METHODOLOGY

The symmetry algorithms applied to large-size color image implies a prohibitive computation time. Currently, computing in Matlab the polygonal symmetry transform on a single 1280×1024 image takes 1273 seconds. Even if an implementation in C may accelerate the process, a pre-selection of connected components based on color and shape information seems to be appropriate. Therefore, our complete pre-detection algorithm consists of three steps: (1) color-based segmentation (2) selection of resulting connected components according to the size, shape and position of the candidates (3) selection by a symmetry criterion.

3.1 Color

In most countries, warning and prohibitory traffic signs have a thick red border, which is a very discriminant characteristic. In the first step of the method, pixels are (individually) classified into red/non-red. An (R, G, B) pixel is considered as red if (Dutilleux and Charbonnier, 2007):

$$R > \alpha(G + B) \quad (1)$$

$$R - \max(G, B) > \beta[\max(G, B) - \min(G, B)]$$

The first expression selects pixels whose normalized red component $R/(R + G + B)$ dominates. Normalization provides robustness to lighting changes. The second expression filters out pixels that tend either

towards yellow or towards magenta (Dutilleux and Charbonnier, 2007). The threshold β has not been empirically determined but we found the rule $\beta = 2\alpha$ satisfactory for all the sequences we encountered. Moreover, our experience is that the best values for α , in terms of classification performance, range between 0.55 and 0.6, the former being a less *selective* value than the latter. An example of red classification map is shown on fig. 1.

3.2 Size, Shape and Position

After pixel classification, red connected components are examined according to several geometric parameters, which reduces the number of candidates.

1. Connected components are first filtered according to their area. The thresholds of course depend on the characteristics of the image acquisition system.
2. The position of the center of mass of the connected component must be in a region-of-interest which correspond to the standard road sign setting in right-hand traffic countries (see Fig. 1).
3. The eccentricity of the components must be smaller than a threshold, whose value results from a trade-off between sensitivity to elongated objects (e.g. poles), that may result in false alarms, and sensitivity to partial occlusions, that decrease the capacity of detection. This value is empirically determined, as explained in Sec. 5.
4. Red connected components that correspond to road signs are relatively empty objects. The extent of a connected component corresponds to the ratio between its area and the area of its bounding box. Bounds on the extent are set by taking margins around the values deduced from norms. This allows distinguishing yield signs from danger signs, for example.
5. In the case of warning signs, the orientation of edges is a discriminant characteristic. The angles between the lateral sides of the connected component and the horizontal are checked. The validity range accounts for a certain margin around the theoretical value of 60° , to provide some flexibility with respect to badly oriented traffic signs.

3.3 Symmetry

The last selection step checks if the remaining connected components are symmetric. To this end, we compute the Fast Radial Symmetry transform (or its extension to polygonal objects) of the luminance image, on a window that corresponds to the bounding



Figure 1: Road scene example (left); red/non-red pixel classification (right). The dotted polygon shows the search region for the selection of connected components. Pixels classified as red are shown in black.

box of each selected component. Checking the symmetry of an object simply amounts to thresholding the resulting vote image. When all connected components have been examined, the image is selected or not, according to the number of remaining objects.

4 EXPERIMENTAL SETUP

4.1 Evaluation Data Sets

In this experimental validation, we consider real-world image sequences acquired by frontal cameras mounted on top of inspection vehicles. The characteristics of the test sequences are given in Tab. 1. Images are taken every 5 or 10 meters, with several kinds of CCD cameras under various, uncontrolled lighting conditions. Note that the evaluation databases comprises about 26,000 images and covers more than 175 km of rural roads, urban roads and highways.

Table 1: Characteristics of the test sequences.

Seq.	Number of images	Step	Camera	Size (pixels)	Size (Ko)
S1	3436	5 m	Basler A101	1280 × 1024	156
S2	3436	5 m	Basler A101	1280 × 1024	156
S3	10420	5 m	Marlin F145-C2	1280 × 1024	95.6
S4	890	10 m	Pike F210-C	1920 × 1080	209
S5	8103	10 m	Pike F210-C	1920 × 1080	223

4.2 Ground Truth

The test sequences were manually processed using a specially designed software to establish a *ground truth*, i.e. to list those images where road signs are visible. Of course, a particular instance of road sign is most of the time visible in several images. We therefore distinguish between the number of traffic signs and the number of images that show traffic signs. These numbers are given in Tab. 2 (WS stands for warning signs and PS stands for prohibitory signs).

Table 2: Ground truth (manual analysis of test sequences).

Seq.	Number of WS	Numb. of images with WS	Number of PS	Numb. of images with PS
S1	25	123	18	93
S2	12	81	5	44
S3	64	383	61	445
S4	9	36	18	63
S5	70	377	89	540
Total	180	1000	191	1185

We note that among the total number of road signs, some of them (about 5% in average) are either worn-out, dirty, badly oriented, or non-standard.

4.3 Evaluation Metrics

To evaluate the performances of the pre-detection system, we use ROC curves, which plot the True Positive Rate (TPR) vs the False Positive Rate (FPR). Each point on a ROC curve corresponds to a particular setting of the detector's parameters. The False Positive Rate is given by:

$$FPR = \frac{FP}{N} \quad (2)$$

where FP is the number of images that contain at least one false alarm. Note that false alarms may occur in images that show a road sign, as soon as the detected component does not fit in the ground-truth bounding box. Hence, N is the total number of images in the sequence.

In our application, it suffices to detect a sign once over the series of images it appears in. Therefore, we define two different true positive rates: the first one, TPR_i , for evaluating the detection of images with traffic signs and the second one, TPR_{rs} , for assessing the detection of road signs. These are defined as:

$$TPR_i = \frac{TP_i}{P_i} \quad \text{and} \quad TPR_{rs} = \frac{TP_{rs}}{P_{rs}} \quad (3)$$

where TP_i is the number of selected images with traffic signs, P_i is the actual number of images with traffic signs, TP_{rs} is the number of detected traffic signs and P_{rs} is the actual number of traffic signs.

5 EXPERIMENTAL RESULTS

In this section, the results on our five test sequences are presented and discussed. Some parameters are *a priori* fixed from theoretical characteristics of traffic signs. For example, the minimum size of connected component is 200 pixels (corresponding to a 30 pixels high object) and the maximum size is 2.5% the image size (the size of the biggest observed sign corresponds

to 1.5% the image size). The upper extent threshold is fixed at 0.35 for the warning signs. The prohibitory signs category includes the “no entry” sign, so the extent threshold is fixed at 0.65 at the risk of a higher false alarm rate. The lower threshold is not used, to accept occluded objects. The validity range for angle in the case of warning signs is set to $[50^\circ, 70^\circ]$.

Sequences S1 and S4 are used to set the value α and the thresholds of eccentricity and symmetry. The algorithm is then tested on sequences S2, S3 and S5.

5.1 Considering Color and Eccentricity

In this series of experiments, the symmetry selection is disabled, to focus on the effect of colour and eccentricity criteria. The influence of the red classification parameter, α and of the eccentricity threshold is illustrated by the ROC curves plotted on fig. 3 for prohibitory signs and on fig. 5 for warning signs. In these experiments, the eccentricity threshold varies over the range $[0.6, 1]$, and α is fixed to 0.55 or 0.6. For both categories, $\alpha = 0.55$ naturally yields more false alarms than $\alpha = 0.6$ but it may also be noticed that the number of true positive is lower. In fact, since more pixels are classified as red when $\alpha = 0.55$, so the red component that corresponds to the sign border may connect with background elements and then, be filtered off by the shape analysis stage. The influence of the color parameter might be worth a more thorough study. However, the value of $\alpha = 0.6$ will be considered in the remaining of the paper.

Concerning eccentricity, the best detection scores are obtained for a threshold of 1, but at the price of a high false alarm rate. When the test becomes more selective, typically for thresholds under 0.85, partly occulted objects are more difficultly detected. Notice that, for prohibitory signs, varying the eccentricity threshold from 0.85 to 0.9 improves the true detection rate faster than the false alarm rate. Moreover, true detection rate almost reaches its maximum for a threshold of 0.9. Hence we retain this value for the rest of our experiments. Similarly, we chose the value of 0.85 in the case of warning signs.

The ROC curves for S4 are easily distinguishable from those corresponding to S1. The false alarm rate is much higher in S4 than in S1. Possible explanations are different cameras, colorization settings, compression rates and nature of scenes (S4 being more urban than S1, for example). This shall be investigated in a near future.

It may be noticed that for prohibitory signs, a 100% true positive rate (TPR_i) is never reached. Some non-detected traffic signs correspond to far-away signs that may be detected when they appear

closer. When TPR_{RS} is considered, the detection rate reaches 94.4% for the S1 sequence (1 road sign is never detected) and 83.3% for the S4 sequence (3 road signs are missed). Non-detected signs correspond to a severely worn-out sign (see Fig. 2(e)) and to signs parallel to the axis of the road. In the case of warning signs, non-detected objects in S1 correspond to old-fashioned, non-standard, worn-out or temporary signs and to one sign with yellow flashes (see Fig. 2(f)). Note that all warning signs are detected in S4.

5.2 Influence of Symmetry

In this experiment, the symmetry threshold varies over the range $[0, 70]$. The value 0 corresponds to no symmetry selection. The resulting ROC curves are plotted on fig. 4 and fig. 6. Examples of good detection, including difficult scenes, are presented on fig. 2(a)-(d). Selection based on symmetry has a noticeable impact on the false alarm rate. This effect is less obvious for warning signs than for prohibitory signs due to a higher extent threshold. However, the initial false positive rate was already weak for warning signs, thanks to a more selective geometrical criterion, namely selection according to angles. Recall that the extent criterion is also more efficient for warning signs than for prohibitory ones. This raises the question of the utility of selection on symmetry, which is rather costly in terms of computation time for polygonal objects, since the number of false positive may already be low for certain sequences.

In general, selection on symmetry tends to discard the first image of the series a road signs appears in, but this has no impact in our application. For circular signs, 3 worn-out “no parking” signs are lost in S1. In France, these signs have a red ring and a blue interior. The lack of contrast between the two colors explain the non-detection. This might be overcome by using other modalities than luminance. For warning signs, selection on symmetry does not decrease the true positive rate TPR_{RS} , except for a high threshold.

In conclusion, selection on symmetry allows strongly decreasing the number of false positives for radial objects. Its interest appears more clearly than for polygonal road signs.

5.3 Validation

The above experiments have lead to the choice of 0.9 for the eccentricity and 40 (resp. 30) for the symmetry threshold in the case of prohibitory (resp. warning) signs. We also take $\alpha = 0.6$, and the other parameters are set as explained at the beginning of sec. 5. In this validation experiment, we apply the detector with the

same set of parameters to sequences S2, S3 and S5. The results are gathered in tab. 3 for prohibitory road signs and in tab. 4 for warning signs.

Table 3: Detection of prohibitory signs (PS).

Seq.	TPR_i	TPR_{rs}	FPR	Rate of selected images
S1	0.67	0.78	0.05	0.07
S4	0.77	0.83	0.175	0.23
S2	1	1	0.015	0.03
S3	0.84	0.9	0.08	0.12
S5	0.86	0.95	0.07	0.12

Table 4: Detection of warning signs (WS).

Seq.	TPR_i	TPR_{rs}	FPR	Rate of selected images
S1	0.77	0.84	0.02	0.05
S4	0.61	1	0.185	0.21
S2	0.88	1	0.01	0.03
S3	0.63	0.875	0.03	0.05
S5	0.67	0.95	0.07	0.11

The results on S2 are similar to those obtained on S1, which was expected since both are part of a single sequence. The results on S5 are even better than those on S4. In fact, the same camera was used, but the acquisition conditions were different and the itinerary is less urban. Results on S3, i.e. with a different camera, that was not involved in the parameter selection process, are of the same quality, which is very satisfactory. The true positive rate is lower than 90% on S3 for warning signs, but this sequence contains more damaged signs and compression artifacts than others.

6 CONCLUSIONS

In this paper we proposed a method for pre-selecting images that potentially contain road signs in large image databases. The method quickly filters objects according to colour, shape, location and symmetry criteria. We applied this algorithm on five large real-world image sequences featuring damaged and badly oriented traffic signs. In general, about 10% images are selected, which fulfills the requirements of our application, and would also be a good starting point for more automatic detection and recognition algorithms (Dutilleux and Charbonnier, 2007) that will hopefully further reduce the false alarm rate. The true detection rates (TPR_{rs}) are quite good on this kind of difficult image sequences: the missed objects always correspond to dirty, worn out or badly oriented traffic signs that sometimes would not be detected by human operators either. We notice that the symmetry algorithm (Barnes et al., 2008) directly applied on the whole image may not detect the damaged traffic signs. Moreover, our complete algorithm takes 3500 sec. to pro-

cess the whole S1 sequence (3436 images) while the symmetry method takes 1200 sec. for one image.

REFERENCES

- Barnes, N., Zelinsky, A., and Fletcher, L. (2008). Real-time speed sign detection using the radial symmetry detector. *IEEE Transactions on Intelligent Transportation Systems*, 9(2):322–332.
- de la Escalera, A., Armingol, J. M., and Mata, M. (2003). Traffic sign recognition and analysis for intelligent vehicles. *Image and Vision Computing*, 21(3):247–258.
- Dutilleux, G. and Charbonnier, P. (2007). Métaheuristiques biologiques pour la détection de la signalisation routière. In Siarry, P., editor, *Optimisation en traitement du signal et de l'image*, Traité IC2, série traitement du signal et de l'image, chapter 10, pages 271–294. Hermes.
- Loy, G. and Barnes, N. (2004). Fast shape-based road sign detection for a driver assistance system. In *IEEE/RSJ International Conference on Intelligent Robots and Systems (IROS'04)*, volume 1, pages 70–75, Sendai, Japan.
- Loy, G. and Zelinsky, A. (2003). Fast radial symmetry for detecting points of interest. *IEEE Transactions on Pattern Analysis and Machine Intelligence*, 25(8):959–973.
- Maldonado-Bascon, S., Lafuente-Arroyo, S., Gil-Jimenez, P., Gomez-Moreno, H., and F.Lopez-Ferreras (2007). Road-sign detection and recognition based on support vector machines. *IEEE Transactions on Intelligent Transportation Systems*, 8(2):264–278.
- Piccioli, G., Micheli, E. D., Parodi, P., and Campani, M. (1996). A robust method for road sign detection and recognition. *Image and Vision Computing Journal*, 14:209–223.
- Priese, L., Rehrmann, V., Schian, R., and Lakmann, R. (1993). Traffic sign recognition based on color image evaluation. In *IEEE Intelligent Vehicles Symposium*, pages 95–100, Tokyo, Japan.
- Shaposhnikov, D., Lubov, N., Podladchikova, L., Golovan, A., Shevtsova, N., Hong, K., and Gao, X. (2002). Road sign recognition by single positioning of space-variant sensor window. In *15th International Conference on Vision Interface*, pages 213–217, Calgary, Canada.

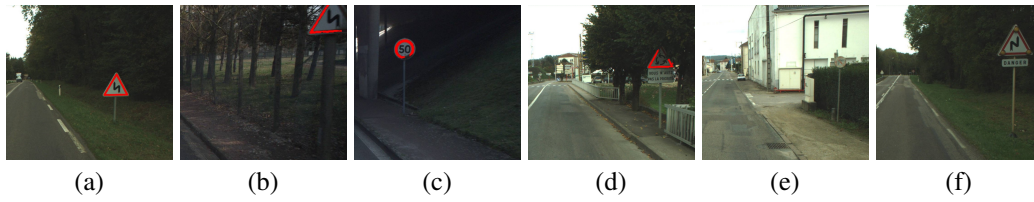


Figure 2: Detection of traffic signs : (a) simple case; (b) old WS ; (c) dirty sign border; (d) occulted WS; (e) severely worn-out PS ; (f) non detected WS with flashes. Detected objects appear in red, superimposed on the original image.

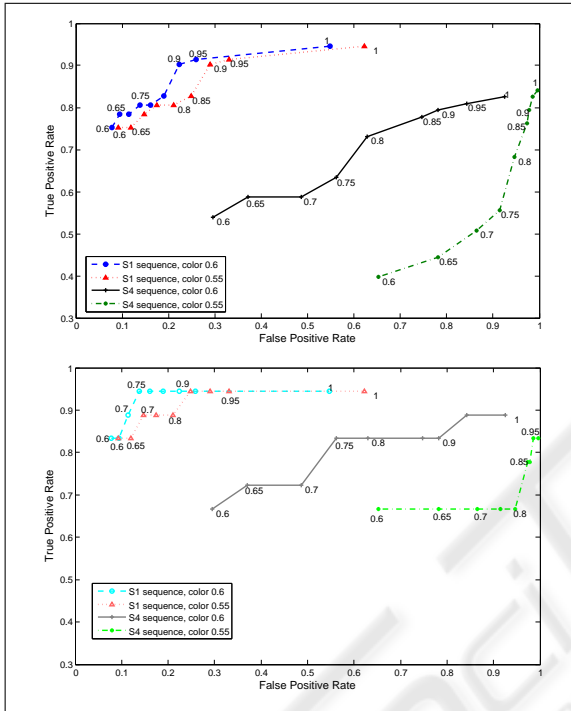


Figure 3: Influence of color and eccentricity parameters on the detection of PS, using TPR_i (top) and TPR_{RS} (bottom); the eccentricity threshold varies over $[0.6, 1]$.

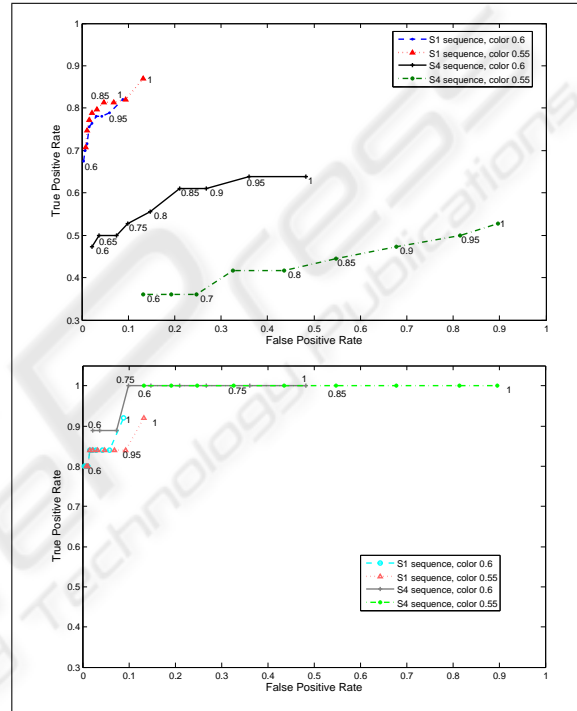


Figure 5: Influence of color and eccentricity parameters on the detection of WS, using TPR_i (top) and TPR_{RS} (bottom); the eccentricity threshold varies over $[0.6, 1]$.

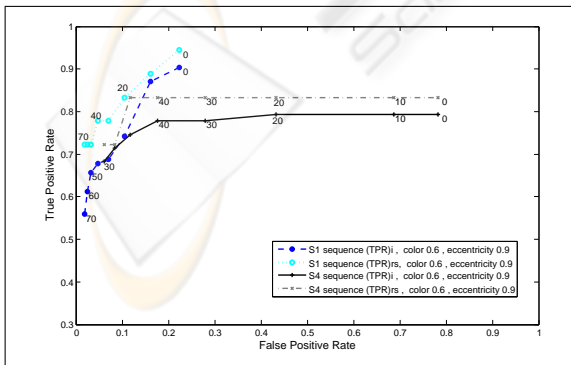


Figure 4: Influence of symmetry on the detection of PS; the symmetry threshold varies over $[0, 70]$.

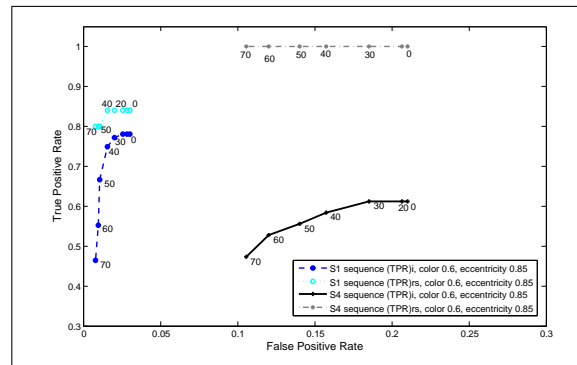


Figure 6: Influence of symmetry on the detection of WS; the symmetry threshold varies over $[0, 70]$. Notice the reduced abscissa range.